RSC Advances

PAPER

View Article Online
View Journal | View Issue

Cite this: *RSC Adv.*, 2025, **15**, 11401

Enhanced peroxidase-like nanozyme: copper-poly(tannic acid) for advanced colorimetric assay of total antioxidant capacity†

Yan Chen, ‡*[ab] Zhaohui Zhang,‡[abc] Yifan Ouyang,[ab] Aikebaier Reheman[ab] and Bei Jiang*[bd]

Received 11th February 2025
Accepted 2nd April 2025

DOI: 10.1039/d5ra00995b

rsc.li/rsc-advances

The assessment of total antioxidant capacity (TAC), a critical marker of food quality in terms of antioxidant efficacy, has garnered considerable attention in human health management. The development of an *in situ* technique that does not require complex apparatus can facilitate accurate and rapid TAC detection. Herein, we developed a specific and sensitive colorimetric assay to evaluate the TAC of fruit juices using the red–green–blue (RGB) model. We synthesized a copper-poly(tannic acid) (Cu-PTA) coordination polymer that exhibits enhanced peroxidase (POD)-like activity in the presence of H_2O_2. This Cu-PTA nanozyme, along with H_2O_2, enhances the conversion of the colorless compound 3,3′,5,5′-tetramethyl-benzidine (TMB) into a visually perceptible oxTMB product. This chromogenic reaction is suppressed in the presence of antioxidants, such as ascorbic acid (AA). This colorimetric assay achieved a limit of detection of 0.06 μM across a concentration range of 0.90–5.40 μM for AA. Our findings enable the development of nanozymes for convenient *in situ* TAC analysis to assess the nutritional value of food items.

1. Introduction

Oxidative stress results from an imbalance between the pro-oxidant and antioxidant levels within an organism, resulting in an elevated oxidation state and subsequent cell damage.[1] Oxidative stress also leads to several diseases, including cardiovascular disease and cancer.[2,3] The consumption of antioxidant-rich food items is crucial for mitigating oxidative stress and the associated health risks.[4] Consequently, the development of a precise, rapid, and convenient method to evaluate the total antioxidant capacity (TAC) of food items has garnered considerable attention. Generally, TAC is a crucial parameter for assessing the antioxidant content.[5] Currently, numerous methodologies exist for determining TAC, including chromatographic, chemiluminescent, and electrochemical techniques.[6–9] Nevertheless, these approaches involve complex equipment and operating procedures. Among these methodologies, colorimetric approaches are more attractive as they are simple and easy to analyze visually.[10,11]

Recently, the enzymatic properties of various nanozymes have been investigated to develop colorimetric methods for TAC detection.[12,13] Nanozymes represent an innovative class of synthetic enzymes that enable biological catalysis. In 2007, Yan and colleagues discovered that ferromagnetic nanoparticles possessed peroxidase (POD)-like activity, providing a basis for nanozyme development.[14] Then, their group established a ferromagnetic nanozyme-based immunoassay platform for the sensitive detection of the SARS-CoV-2 antigen.[15] Nanozymes have several benefits over natural enzymes, including low cost, excellent stability, extended storage duration, and facile surface modification.[16] Therefore, engineering a nanozyme exhibiting high catalytic activity can be adaptively employed to analyze food products. To date, numerous nanomaterials have been identified that exhibit pronounced POD-like activities, including noble metals,[17] metal oxides,[18] carbon-based nanomaterials,[19,20] and metal–organic frameworks (MOFs).[21–23] As a central active metal component in natural proteins and enzymes, copper-based nanozymes have gained considerable attention.[24]

Herein, we developed a formaldehyde-mediated metal–ligand crosslinking strategy for fabricating a copper-poly(tannic acid) (Cu-PTA)-coordinated polymer based on sol–gel chemistry. The coordination of Cu^{2+} with PTA results in a Cu–O–C structure, similar to a natural heme enzyme.[25,26] The three-dimensional network structure of PTA is cross-linked through hydrogen bonds and intermolecular forces, reducing the risk of metal ion detachment. Besides, compared with tannic acid(TA), the long-chain PTA molecules possess significantly more phenolic hydroxyl groups, which would improve the loading

[a]*Fujian Key Laboratory of Toxicant and Drug Toxicology, Ningde Normal University, Ningde, Fujian, China. E-mail: chenyan@ndnu.edu.cn*

[b]*Medical School, Ningde Normal University, Ningde, Fujian, China*

[c]*Department of Chemistry, Fuzhou University, Fuzhou, Fujian, China*

[d]*Yunnan Key Laboratory of Screening and Research on Anti-pathogenic Plant Resources from Western Yunnan, Dali, China. E-mail: dalinorthjiang@163.com*

† Electronic supplementary information (ESI) available. See DOI: https://doi.org/10.1039/d5ra00995b

‡ The authors contributed equally to this work.

capacity. This long molecular chains of PTA also could act as "conductive bridges", accelerating the transfer of electrons from the substrate to the active sites, which enhanced electron conduction.[27,28] These Cu-PTA conjugates showed excellent POD-like characteristics and can produce reactive oxygen species (ROS). Through this mechanism, the Cu-PTA nanozyme facilitates the transformation of a colorless compound 3,3′,5,5′-tetramethyl-benzidine (TMB) into the visually detectable blue oxTMB substrate in the presence of H_2O_2. The introduction of antioxidants, like ascorbic acid (AA), inhibits this chromogenic reaction. Thus, the POD-like activity of the Cu-PTA nanozyme forms the underlying mechanism for establishing a colorimetric assay to measure the TAC (Scheme 1). The TAC values were obtained by taking pictures of the detection solution containing antioxidants, such as AA, and analyzing them using a red–green–blue (RGB) model. This method was further used to detect the TAC of fruit juices, providing potential insights into developing a portable on-site TAC detection system.

2. Experimental section

2.1 Chemicals and characterization

3,3′,5,5′-Tetramethylbenzidine (TMB), L-ascorbic acid (AA), tertiary-butyl alcohol (TBA), and $CuCl_2 \cdot 2H_2O$ were purchased from Macklin Biochemical Co., Ltd. Benzoquinone (*p*-BQ), L-histidine (L-His), tannic acid (TA, analytical regent) and 1,2-diaminobenzene (OPD) were bought from Adamas Co., Ltd. Formaldehyde (CH_2O, 37%) and ammonium hydroxide (25%) were obtained from Xilong technology Company. 2,2′-Azinobis(3-ethylbenzothiazoline-6-sulfonic acid) (ABTS) bought from Aladdin company. Fruits (orange, grape, kiwi, pomegranate) were bought from the local market. The lycine (Gly), threonine (Thr), lysine (Lys), glutamic acid (Glu), histidine(His), phenylalanine (Phe), leucine (Leu), isoleucine (Ile) and tryptophan (Try), with HPLC grade, bought from Beijing Solaibao Technology Co., Ltd. Fructose (99%), sucrose (>99.0%), lactose (98%), glucose (>99.5%), $MgCl_2$ (>99.0%) and dopamine (DA, >99.0%) bought from Adamas. The maltose (>95%) bought from Shanghai Haohong Biomedical Technology Co., Ltd. NaCl (AR) bought from Xilong Kexue Co., Ltd. KOH (AR) bought from Tianjing Hengxing chemical Co., Ltd.

The SEM micrographs were recorded on GeminiSEM 300. UV-vis spectra were recorded on a SHIMADZU UV-1780 spectrophotometer and microplate reader from Meigu Molecular Devices Company (CMax Plus). Electron spin resonance (ESR) spectra were got from Bruker EMXplus-6/1 (Germany). Fourier transform infrared spectra (FTIR) were measured by Thermo Fisher Scientific Nicolet iS20 (USA). The X-ray diffraction (XRD) spectra were got from Rigaku SmartLab SE (Japan). The X-ray photoelectron spectroscopy (XPS) obtained from Thermo Scientific K-Alpha (USA).

2.2 Synthesis of Cu-PTA

Firstly, 0.2 g F127 was dissolved in 46 mL water and 8 mL ethanol. Then we added 0.5 mL ammonia solution (25 wt%) and stired for 1 hour. Then 0.2 g tannic acid was added to the above solution. After the tannic acid was completely dissolved, 0.38 mL of formaldehyde solution (37 wt%) was added. After stirring for 24 hours, $CuCl_2$ solution (0.1g $CuCl_2 \cdot 2H_2O$ dissolved in 2 mL water) was added. After stirring for 24 hours, the product was transferred to a 100 mL high-pressure reactor and hydrothermally treated at 100 °C for another 24 hours. The obtained metal-poly(tannic acid) nanozyme (Cu-PTA) was collected by centrifugation and washing. Finally, the prepared Cu-PTA nanozyme was ultrasonically dispersed into ultrapure water for future use.

2.3 POD activity of Cu-PTA nanozyme

The POD activity of the synthesized Cu-PTA nanozyme was analyzed using TMB as the chromogenic substrate. The specific steps were as follows: 20 μL of Cu-PTA nanozyme (0.9 mg mL^{-1}), 100 μL of H_2O_2 (25 mM) and 100 μL of TMB (10 mM) were added to 780 μL of NaAc/HAc buffer (100 mM, pH 5.0). After incubation at 37 °C for 5 min, the absorbance of the reaction system was recorded by an UV-vis spectrophotometer. For the control group, 20 μL 0.9 mg mL^{-1} Cu-PTA nanozyme was replaced with the same volume of NaAc/HAc buffer, and the detection process was the same as above. For other chromogenic substrate groups, the TMB was replaced with OPD or ABTS at the same concentration, and the experimental procedures were the same as described above.

2.4 AA detection

AA detection was conducted on 96-well plates by following steps: 5 μL Cu-PTA nanozyme (0.9 mg mL^{-1}), 50 μL H_2O_2 (25

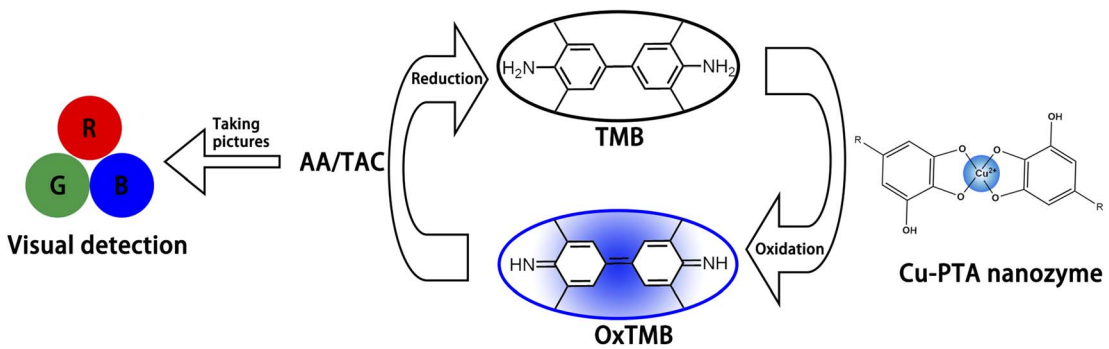

Scheme 1 Colorimetric assay of the total antioxidant capacity using the Cu-PTA nanozyme.

mM), and 25 μL TMB solution (10 mM) were added to 150 μL NaAc/HAc buffer (100 mM, pH 5.0). The absorption was measured by microplate reader at 652 nm. After AA addition (50 μL) and incubated at 37 °C for 5 min, the absorbance of ox-TMB at 652 nm was recorded as A. When the AA solution replaced with 200 μL of NaAc/HAc buffer solution, the absorbance at 652 nm was set as A_0. In addition, the condition of pH, temperature, concentration of Cu-PTA nanozyme and H_2O_2 were optimized to get highest signal.

Commercially available fresh fruits were squeezed by juice extractor. Then the TAC assay of fruit juices (orange juice, grape juice, kiwi juice, pomegranate juice) were diluted before detection. The procedures were the same as AA detection. The RGB values were extracted by ImageJ with the function of pixel inspector.

2.5 Analysis of enzymatic reaction kinetics

The catalytic reaction rate of nanozyme is affected by the activity of nanozyme. The steady-state kinetics of the enzymatic reaction of Cu-PTA nanozymes was studied by changing the concentration of TMB or H_2O_2. Firstly, the reaction kinetics of Cu-PTA nanozyme on the substrate TMB was investigated, while the concentration of H_2O_2 kept constant. The procedure was as follows: 200 μL NaAc/HAc buffer (100 mM pH 5.0), 5 μL Cu-PTA nanozyme (0.9 mg mL^{-1}), 50 μL H_2O_2 solution (25 mM) and 25 μL TMB solution (0.1–1.2 mM) were added into 96-well plate. The absorbance at 0 s and 60 s were recorded by microplate reader. Secondly, the reaction kinetics of Cu-PTA nanozyme on the substrate H_2O_2 (1–600 mM) was investigated, while the concentration of TMB kept constant. The absorbance of the reaction system at 0 s and 60 s was recorded immediately.

The initial reaction rate (V_0) was calculated according to eqn (1) and (2).

$$A = \varepsilon bc \quad (1)$$

$$V_0 = \Delta c/\Delta t \quad (2)$$

where A is the absorbance at 652 nm, c is the concentration of the substrate (H_2O_2 or TMB), b is the depth of detection penetration (0.8 cm); ε is the molar absorption coefficient of TMB (39 000 M cm^{-1}), V_0 is the initial reaction rate (M s^{-1}).

The Michaelis–Menten eqn (3), expressed the relationship between the initial velocity of enzymatic reaction and the concentration of the substrate to describe the metabolic kinetics. According to the double-reciprocal plot, we can calculate the value of Michaelis constant (Km) and maximum reaction velocity (V_{max}), respectively.

$$V_0 = (V_{max} \times [s])/((K_m + [s])) \quad (3)$$

$$\frac{1}{V_0} = \frac{K_m}{V_{max}}\left(\frac{1}{[s]} + \frac{1}{K_m}\right) \quad (4)$$

2.6 Analysis of recyclability and stability

For the recyclability analysis: 20 μL of Cu-PTA nanozyme (0.9 mg mL^{-1}), 100 μL of H_2O_2 (25 mM), 100 μL of TMB (10 mM), and 200 μL of 1 mM AA were added into the NaAc/HAc buffer solution (pH 5.0, 100 mM), with a total volume of 1 mL. The blank control is A_0, which replaced the AA solution with 200 μL of NaAc/HAc buffer solution. Then the mixture was vibrated at 37 °C for 5 min. The absorption at the wavelength of 652 nm was recorded immediately. After that, the Cu-PTA nanozyme was purified by following procedure: the mixture was washed with methanol, and centrifuged (9000 rpm, 10 min) for several times. The resulted precipitate was dissolved in 20 μL of ultrapure water, and carried out for the next cycle. For the stability analysis: the analysis was conducted on 96-well plate, and the procedure was the same as AA detection, except that Cu-PTA nanozyme was stored for certain time period before used in AA detection.

3. Results and discussion

3.1 Synthesis and characterization of the Cu-PTA nanozymes

Herein, we introduced metal polyphenol coordination spheres integrating Cu^{2+} with TA based on the principle of sol–gel chemistry.[27] The TA was first crosslinked using formaldehyde in an alkaline ethanol/water solution. Then, the metal species Cu^{2+} was introduced to incorporate the polyphenol colloidal sphere framework. After vigorous stirring for 24 h, the solution was transferred to a steel reactor and treated at 100 °C for 24 h to increase the stability of the Cu-PTA nanozyme (Scheme 2). The morphology and crystallinity of the Cu-PTA nanozyme were characterized. As seen from Fig. 1A, B and S1,† the rough surface of the Cu-PTA nanozyme may contribute to its excellent POD-like activity. The rough surface facilitate active site exposure, as well as substrate (like H_2O_2 and TMB) concentration and adsorption. The rough surface's tortuous pathways and interconnected pores facilitate efficient electron transfer between the active site and substrate.[29,30] The Cu-PTA nanozyme had a mean particle diameter of 90.15 nm, as shown by dynamic light scattering (DLS) results (Fig. 1C), and exhibited excellent water dispersibility (Fig. S12†). Energy-dispersive X-ray spectroscopy (EDS) of Cu-PTA nanozyme proved the existence of C, N, O, and Cu, which were uniformly distributed on the surface of this nanozyme (Fig. 1D). The existence of N element in the Cu-PTA nanozyme, indicated that a part of hydroxyl groups from PTA was possibly replaced by the amino group when using $NH_3 \cdot H_2O$ as a N source during the synthesis process.[31,32]

The coordination between Cu^{2+} and PTA was confirmed by FTIR, XRD and XPS, respectively (Fig. S2–S4†). Due to the coordination to Cu^{2+}, the resultant Cu-PTA nanozyme showed shifting of absorption in the FTIR spectrum when compared with PTA itself. The shifting of absorption in the fingerprint region indicated the disruption of HO–C vibration of PTA after coordinating with Cu^{2+} by the phenolic groups. According to the XRD results, both Cu-PTA and PTA showed amorphous framework. Furthermore, the oxidation state of Cu(I) and Cu(II) was revealed by XPS. The coordination between Cu^{2+} and PTA stabilizes reactive intermediates and facilitates electron transfer during catalysis.

3.2 Enzyme mimetic activities of the Cu-PTA nanozyme

Three commonly used chromogenic substrates (TMB, OPD and ABTS) were selected to investigate the POD-mimicking ability of

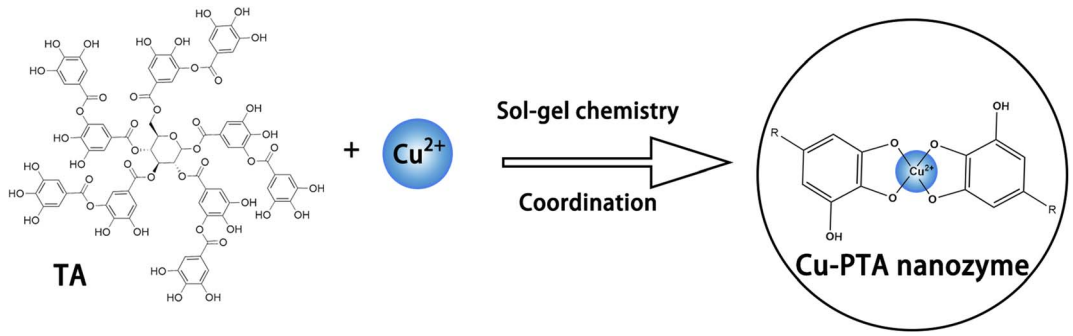

Scheme 2 Preparation method of the Cu-PTA nanozyme.

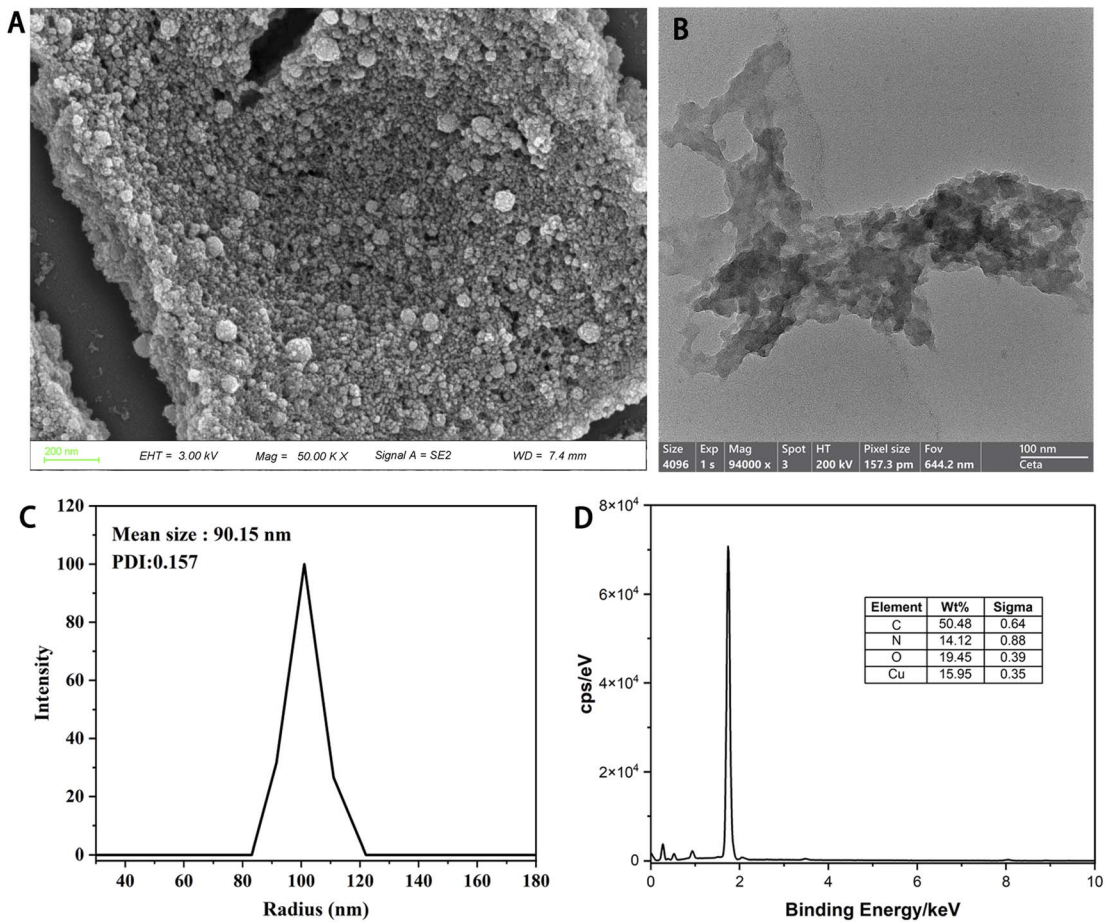

Fig. 1 Characterization of the Cu-PTA nanozyme using SEM (A), TEM (B), DLS (C), and SEM-EDS (D).

the Cu-PTA nanozyme. As shown in Fig. 2A, when these substrates were oxidized to oxTMB, oxOPD, and oxABTS, the color of the solution turned blue, yellow, and green, respectively. This indicated that the Cu-PTA nanozyme has enzyme-mimicking abilities and could oxidize the POD-like chromogenic substrates. However, as the absorption of oxTMB was substantially higher at a wavelength of 652 nm compared with the other substrates, TMB was selected as the chromogenic substrate for subsequent experiments.

The POD activity of the Cu-PTA nanozyme was further verified *via* UV-vis absorption with different groups. As shown in Fig. 2B, the TMB, TMB/H_2O_2, and TMB/Cu-PTA groups were colorless and had no characteristic absorption peaks. However, when H_2O_2 and the Cu-PTA nanozyme were added together, TMB was oxidized to the blue-colored oxTMB, resulting in an obvious absorption peak at 652 nm. This proved that H_2O_2 is required for the POD-mimicking activity of Cu-PTA. The Cu-PTA nanozyme plays a crucial role in the oxidation of TMB. Its POD-like activity enables the conversion of TMB into the detectable product oxTMB in the presence of H_2O_2, and this process is fundamental for the colorimetric assay of total antioxidant capacity.

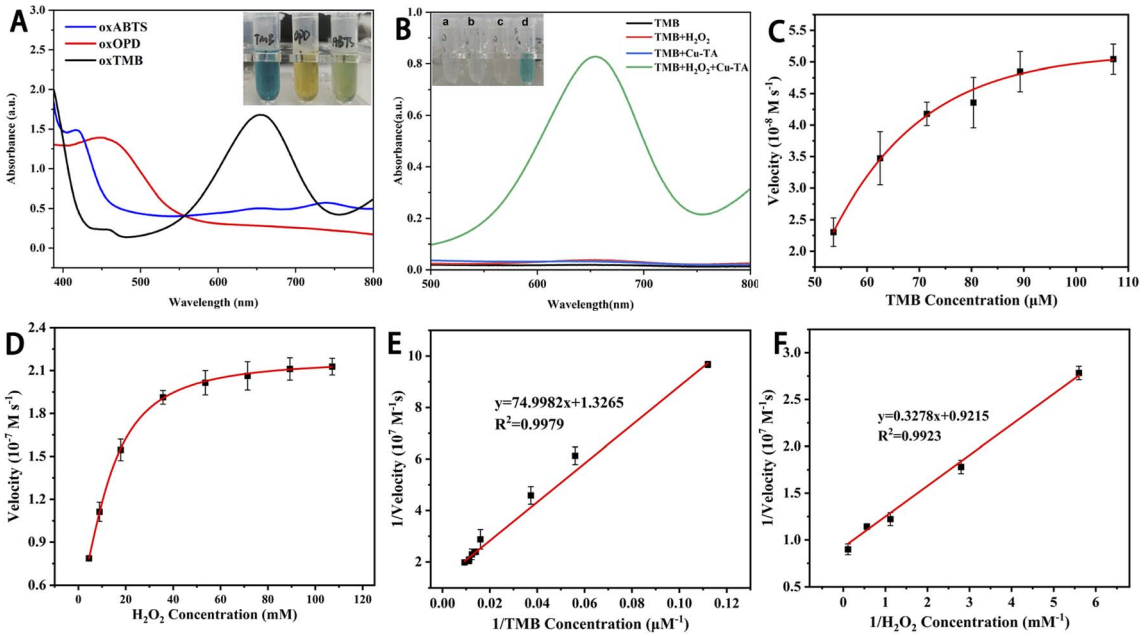

Fig. 2 (A) UV-vis absorption spectra of the Cu-PTA catalyzed oxidation of ABTS, OPD, and TMB. (B) Colorimetric signals of various reaction systems and inset picture from left to right: TMB (A), TMB + H_2O_2 (B), TMB + Cu-PTA (C), and TMB + H_2O_2 + Cu-PTA (D). Michaelis–menten curve fitted for TMB (C) and H_2O_2 (D). Lineweaver–Burk plot for TMB (E) and H_2O_2 (F). Each error bar represents the SD of three independent measurements.

3.3 Kinetics and catalytic mechanism of the Cu-PTA nanozyme

Typical Michaelis–Menten curves were obtained at the appropriate concentration range of TMB and H_2O_2 (Fig. 2C and D). The Lineweaver–Burk double reciprocal curves of TMB and H_2O_2 (Fig. 2E and F) showed that the catalytic reaction followed the Michaelis–Menten model. For TMB and H_2O_2, the calculated K_m values were 0.0565 and 0.356 mM, respectively, while their V_{max} values were 7.54×10^{-8} and 10.85×10^{-8} M s^{-1}, respectively. The K_m for TMB was lower than that of H_2O_2, indicating that the Cu-PTA nanozyme has a higher affinity to TMB than to H_2O_2. Further, the K_m and V_{max} values of Cu-PTA for TMB and H_2O_2 were close to that of horse radish peroxidase and other POD-like nanozyme (Table S1†). This data shows that the Cu-PTA nanozyme had high affinity and catalytic efficiency, validating its excellent POD-like activity. Therefore, this nanozyme can be a superior alternative to natural enzymes for colorimetric detection.

To further explore the catalytic mechanism of the POD-like activity of the Cu-PTA nanozymes, the different ROS types generated during the reaction were studied. According to the electron paramagnetic resonance (EPR) spectra (Fig. 3 and S5†), the Cu-PTA-H_2O_2-dimethyl-1-pyrroline-*N*-oxide (DMPO) system displays high signal of DMPO-˙OH. The quenching agents of TBA, p-BQ, and L-His were used to scavenge ˙OH, $O_2^{\cdot-}$ and $^1O_2$, respectively. The data showed that TBA got big influence on the TMB oxidation, which indicated that ˙OH is the main ROS (Fig. S6†). The results indicated that the POD-like activity of Cu-PTA primarily produces ˙OH, which subsequently oxidizes TMB.

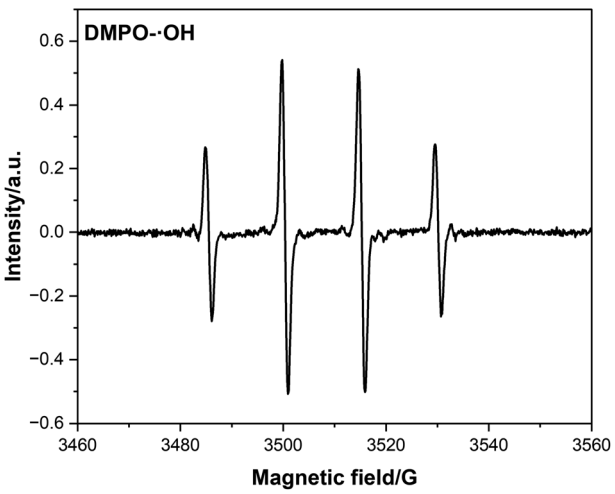

Fig. 3 EPR spectra with the spin trapping of 5,5-dimethyl-1-pyrroline n-oxide (DMPO) for ˙OH in the Cu-PTA system (H_2O_2 = 10 mM).

3.4 Detection of the antioxidants

The ROS produced by the Cu-PTA nanozyme oxidizes TMB to oxTMB. Antioxidants inhibit this process, leading to a decline in the UV-vis absorbance. Based on this principle, AA was selected to evaluate the feasibility of TAC detection. The results showed that when the AA concentration was fixed at 0.18 mM, the signal for AA was highly notable at a pH of 5, 37 °C and Cu-PTA nanozyme and H_2O_2 concentrations of 16 μg mL^{-1} and 4.46 mM, respectively (Fig. S7–S10†). Therefore, we used these optimal conditions for subsequent experiments.

AA and the corresponding absorbance $(A_0 - A)/A_0$ in the range of 0.90–5.40 μM displayed a good linear relation with a linear correlation coefficient (R^2) of 0.9968 (Fig. 4A). According to the three times signal-to-noise ratio, the detection limit (LOD) for AA was 0.06 μM. The linear range and LOD were comparable with other reported nanozymes, which showed its broad application for AA detection (Table S2†). Further, AA was detected based on the color intensity of the reaction solution. Pictures of this solution were captured using a smartphone and then processed using the ImageJ software to extract the red (R), green (G), and blue (B) values. The AA concentration and *R*-value exhibited a good linear relation with an R^2 value of 0.9911 (Fig. 4B and C). Therefore, the visual detection of AA can be realized by simply taking pictures without involving large equipment.

Then, the inhibition mechanism of the antioxidant AA was explored. When the AA concentration increased, the slope of the curve remained unchanged, but the increase in absorption was delayed (Fig. 4D). This inhibition might because the ROS produced by Cu-PTA nanozyme was more likely reacted with AA, resulting in a delay in the reaction with TMB. However, since the catalyst was not consumed or poisoned in this process, the plot slopes were the same as those without AA.[33]

Several potentially interfering substances, such as amino acids, carbohydrates, and metal ions, were introduced to evaluate the selectivity and the anti-interference ability of the sensor system. As shown in Fig. 4E, the AA group showed much higher corresponding absorbance compared with the interfering substances. AA has a specific enediol structure, which gives it strong reducibility. Due to this unique chemical structures, other substances showed limited reducibility, resulting in little interference. The results proved that the sensor system had high selectivity and strong anti-interference ability for detecting AA. Moreover, we conducted the recyclability and stability tests, and it turned out that the Cu-PTA nanozyme survived three times of cyclic AA detection (Fig. S11A†). The Cu-PTA aqueous solution, which stored for 30 or 60 days, did not show much precipitation and was quite stable (Fig. S12†). In addition, the stored Cu-PTA nanozyme did not show much attenuation for AA detection (Fig. S11B†).

3.5 TAC assay using fruit juices

TAC detection has gained considerable interest in food engineering. Even at a low concentration, the TAC prevents the action of free radicals. Therefore, TAC can be used to estimate the antioxidants and their comprehensive parameters in actual fruit samples. Herein, AA was selected as an antioxidant, which delayed the color change of the TMB–H_2O_2 system catalyzed by the Cu-PTA nanozyme. In addition, the TAC detection based on the RGB model as established. First, the photos of the detection samples were captured using a smartphone and converted into the RGB color intensity values using the ImageJ software. As the *R* intensity values showed an excellent linear relation with the AA concentration, we were able to evaluate the exact AA concentration in actual samples. Thus, this detection method can be widely and conveniently used for *in situ* TAC assay. Further, the TAC of four freshly squeezed fruit juices a was detected and analyzed to verify the practical feasibility and accuracy of the detection method. The TAC in orange, grape, kiwi, and pomegranate juices were detected by the linear plot of

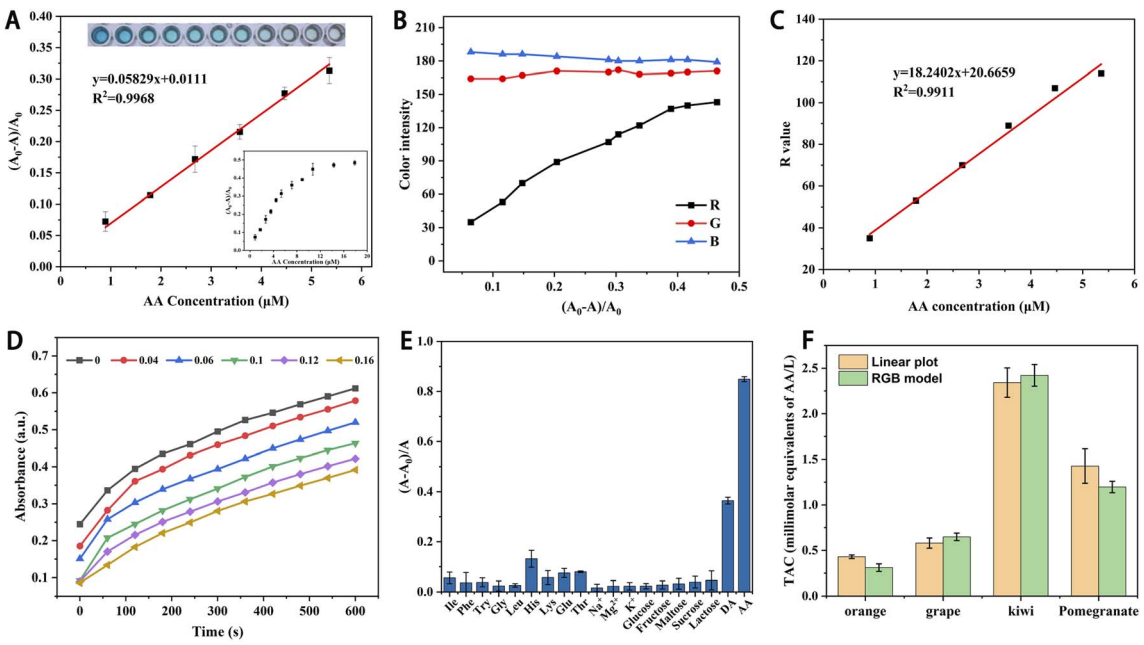

Fig. 4 (A) Linear plots of the relative absorbance *versus* the concentrations of AA. (B) The RGB values during the relative absorbance changes. (C) The linear plot of aa concentration with the *R* intensity value acquired by the RGB model. (D) Time-dependent absorbance at 652 nm of the Cu-PTA–H_2O_2 system containing varying AA concentrations. (E) The absorbance of the Cu-PTA–H_2O_2 system at 652 nm after adding interfering substances ([AA] = 1 mM, [DA] = 1 mM, the other interfering substances were 5 mM). (F) TAC detection in different fruit juices. Each error bar represents the SD of three independent measurements.

AA and RGB model, respectively (Fig. 4F). The kiwi juice displayed the highest antioxidant activity. These results showed that TAC detection can potentially be applied to test other food samples by RGB model in a convenient way.

In this catalytic process, The Cu-PTA nanozyme catalyzes the decomposition of H_2O_2 to generate $^{\bullet}OH$, which are the reactive species responsible for oxidizing TMB. The generated $^{\bullet}OH$ radicals react with TMB, oxidizing it to oxTMB, which exhibits a distinct blue color and a strong absorption peak at 652 nm in UV-vis spectroscopy. This chromogenic reaction forms the basis of the colorimetric assay for TAC detection. When antioxidants are present, they inhibit this reaction, which can be used to evaluate the TAC of samples.

4. Conclusion

Herein, a Cu-PTA nanozyme was synthesized based on the principle of sol–gel chemistry. The hydroxyl radical ($^{\bullet}OH$) were crucial for the POD-like activity of the Cu-PTA nanozyme, which effectively oxidized the chromogenic substrate TMB into oxTMB. This process was interrupted by antioxidants, such as AA. Further, we developed an innovative colorimetric assay for assessing TAC based on the POD-like catalytic activity of the Cu-PTA nanozyme, which could be visualized using the RGB model. The pH values, temperature, the Cu-PTA nanozyme and H_2O_2 concentrations in the Cu-PTA-H_2O_2–TMB detection system were optimized to obtain a high signal. A steady-state kinetic study of the enzymatic reaction showed that the Cu-PTA nanozyme had good affinity and catalytic efficiency for TMB and H_2O_2 substrates. In addition, this TAC colorimetric assay exhibited high anti-interference ability. Using AA as a TAC detection model, this method was employed to ascertain TAC in fruit juices, yielding satisfactory results. By capturing images of the reaction solution with a smartphone and analyzing the RGB values (especially the red channel intensity), the TAC concentration can be quantified without requiring bulky instruments. These features collectively enable the development of a low-cost, user-friendly portable platform for antioxidant analysis in food and biological samples.

Data availability

The data supporting this article have been included as part of the ESI.†

Author contributions

Y. Chen and Z. Zhang contributed equally to this work. Y. Chen: data curation, supervision, funding acquisition, project administration, review & editing. Z. Zhang: investigation, data curation, writing original draft. Y. Ouyang: data curation. A. Reheman: conceptualization. B. Jiang: conceptualization, supervision, formal analysis, project administration.

Conflicts of interest

There are no conflicts to declare.

Acknowledgements

The authors extend their gratitude to Ms. Yinghua Chi from Shiyanjia Lab (https://www.shiyanjia.com) for providing invaluable assistance with the TEM analysis. This work was supported by Innovation Team project of Ningde Normal University (2022T03, 2023T05), Natural Science Foundation of the Fujian Province (2022J05277), and Scientific Research Fund project of Ningde Normal University (2018Y01, 2022Y13, 2022Y18).

References

1 H. Sies, Oxidative stress: concept and some practical aspects, *Antioxidants*, 2020, **9**, 852, DOI: 10.3390/antiox9090852.
2 H. Choi, B. Choi, J. H. Han, H. E. Shin, W. Park and D. H. Kim, Reactive oxygen species responsive cleavable hierarchical metallic supra-nanostructure, *Small*, 2022, **18**, e2202694, DOI: 10.1002/smll.202202694.
3 G. Pizzino, N. Irrera, M. Cucinotta, G. Pallio, F. Mannino, V. Arcoraci, F. Squadrito, D. Altavilla and A. Bitto, Oxidative stress: harms and benefits for human health, *Oxid. Med. Cell. Longev.*, 2017, **2017**, 8416763, DOI: 10.1155/2017/8416763.
4 L. Fu, B. Xu, X. Xu, R. Gan, Y. Zhang, E. Xia and H. Li, Antioxidant capacities and total phenolic contents of 62 fruits, *Food Chem.*, 2011, **129**, 345–350, DOI: 10.1016/j.foodchem.2011.04.079.
5 C. G. Fraga, P. I. Oteiza and M. Galleano, *In vitro* measurements and interpretation of total antioxidant capacity, *Biochim. Biophys. Acta Gen. Subj.*, 2014, **1840**, 931–934, DOI: 10.1016/j.bbagen.2013.06.030.
6 X. Zhang, Z. Lin, J. Fang, M. Liu, Y. Niu, S. Chen and H. Wang, An on-line high-performance liquid chromatography-diode-array detector-electrospray ionization-ion-trap-time-of-flight-mass spectrometry-total antioxidant capacity detection system applying two antioxidant methods for activity evaluation of the edible flowers from *Prunus mume*, *J. Chromatogr. A*, 2015, **1414**, 88–102, DOI: 10.1016/j.chroma.2015.08.033.
7 G. K. Pamunuwa and S. N. Atapattu, Chemiluminescence methods for antioxidant analysis in food matrices, *J. Chromatogr. Open*, 2023, **4**, 100096, DOI: 10.1016/j.jcoa.2023.100096.
8 S. Meneses, K. Marques, C. Pires, J. Santos, E. Fernandes, J. Lima and E. Zagatto, Evaluation of the total antioxidant capacity by using a multipumping flow system with chemiluminescent detection, *Anal. Biochem.*, 2005, **345**, 90–95, DOI: 10.1016/j.ab.2005.07.017.
9 M. A. Haque, K. Morozova, G. Ferrentino and M. Scampicchio, Electrochemical methods to evaluate the antioxidant activity and capacity of foods: a review, *Electroanalysis*, 2021, **33**, 1419–1435, DOI: 10.1002/elan.202060600.
10 Y. Miao, M. Xia, C. Tao, J. Zhang, P. Ni, Y. Jiang and Y. Lu, Iron-doped carbon nitride with enhanced peroxidase-like activity for smartphone-based colorimetric assay of total

antioxidant capacity, *Talanta*, 2024, **267**, 125141, DOI: 10.1016/j.talanta.2023.125141.

11 H. Wu, J. Chen, P. Lin, Y. Su, H. Li, W. Xiao and J. Peng, Nanozyme-catalyzed colorimetric detection of the total antioxidant capacity in body fluids by paper-based microfluidic chips, *ACS Appl. Mater. Interfaces*, 2024, **16**, 39857–39866, DOI: 10.1021/acsami.4c07835.

12 T. Wang, J. Feng, H. Sun, Y. Liang, T. Du, J. Dan, J. Wang and W. Zhang, CuBi bimetallic aerogel as peroxidase-like nanozyme for total antioxidant capacity colorimetric detection, *Sens. Actuators, B*, 2023, **379**, 133249, DOI: 10.1016/j.snb.2022.133249.

13 J. Li, Y. Zhou, Y. Xiao, S. Cai, C. Huang, S. Guo, Y. Sun, R. Song and Z. Li, Carbon dots as light-responsive oxidase-like nanozyme for colorimetric detection of total antioxidant capacity in fruits, *Food Chem.*, 2023, **405**, 134749, DOI: 10.1016/j.foodchem.2022.134749.

14 L. Gao, J. Zhuang, L. Nie, J. Zhang, Y. Zhang, N. Gu, T. Wang, J. Feng, D. Yang, S. Perrett and X. Yan, Intrinsic peroxidase-like activity of ferromagnetic nanoparticles, *Nat. Nanotechnol.*, 2007, **2**, 577–583, DOI: 10.1038/nnano.2007.260.

15 D. Liu, C. Ju, C. Han, R. Shi, X. Chen, D. Duan, J. Yan and X. Yan, Nanozyme chemiluminescence paper test for rapid and sensitive detection of SARS-CoV-2 antigen, *Biosens. Bioelectron.*, 2021, **173**, 112817, DOI: 10.1016/j.bios.2020.112817.

16 M. Liang and X. Yan, Nanozymes: from new concepts, mechanisms, and standards to applications, *Acc. Chem. Res.*, 2019, **52**, 2190–2200, DOI: 10.1021/acs.accounts.9b00140.

17 M. Dadmehr, M. Mortezaei and B. Korouzhdehi, Dual mode fluorometric and colorimetric detection of matrix metalloproteinase MMP-9 as a cancer biomarker based on AuNPs@gelatin/AuNCs nanocomposite, *Biosens. Bioelectron.*, 2023, **220**, 114889, DOI: 10.1016/j.bios.2022.114889.

18 W. Yang, C. Weng, X. Li, H. He, J. Fei, W. Xu, X. Yan, W. Zhu, H. Zhang and X. Zhou, A sensitive colorimetric sensor based on one-pot preparation of h-Fe_3O_4@ppy with high peroxidase-like activity for determination of glutathione and H_2O_2, *Sens. Actuators, B*, 2021, **338**, 129844, DOI: 10.1016/j.snb.2021.129844.

19 X. Liu, Y. Jiao, Y. Zheng, M. Jaroniec and S. Qiao, Building up a picture of the electrocatalytic nitrogen reduction activity of transition metal single-atom catalysts, *J. Am. Chem. Soc.*, 2019, **141**, 9664–9672, DOI: 10.1021/jacs.9b03811.

20 P. Zhang, D. Sun, A. Cho, S. Weon, S. Lee, J. Lee, J. W. Han, D. P. Kim and W. Choi, Modified carbon nitride nanozyme as bifunctional glucose oxidase-peroxidase for metal-free bioinspired cascade photocatalysis, *Nat. Commun.*, 2019, **10**, 940, DOI: 10.1038/s41467-019-08731-y.

21 X. Huang, S. Zhang, Y. Tang, X. Zhang, Y. Bai and H. Pang, Advances in metal-organic framework-based nanozymes and their applications, *Coord. Chem. Rev.*, 2021, **449**, 214216, DOI: 10.1016/j.ccr.2021.214216.

22 R. Jesuraj, A. Amalraj, V. K. Vaidyanathan and P. Perumal, Exceptional peroxidase-like activity of an iron and copper based organic framework nanosheet for consecutive colorimetric biosensing of glucose and kanamycin in real food samples, *Analyst*, 2023, **148**, 5157–5171, DOI: 10.1039/D3AN01242E.

23 A. Amalraj, M. Narayanana and P. Perumal, Highly efficient peroxidase-like activity of a metal–oxide-incorporated CeO_2-MIL(Fe) metal–organic framework and its application in the colorimetric detection of melamine and mercury ions *via* induced hydrogen and covalent bonds, *Analyst*, 2022, **147**, 3234–3247, DOI: 10.1039/D2AN00864E.

24 J. Niu, S. Sun, P. Liu, X. Zhang and X. Mu, Copper-based nanozymes: properties and applications in biomedicine, *Inorg. Mater.*, 2023, **38**, 489–502, DOI: 10.15541/jim20220716.

25 T. L. Poulos, Heme enzyme structure and function, *Chem. Rev.*, 2014, **114**, 3919–3962, DOI: 10.1021/cr400415k.

26 Y. Huang, H. Zhong, C. Jiang, J. Yang, J. Zhang, F. Zhao and C. Liu, Copper-based nanomaterials as peroxidase candidates for intelligent colorimetric detection and antibacterial applications, *Particuology*, 2024, **84**, 126–135, DOI: 10.1016/j.partic.2023.03.009.

27 J. Wei, G. Wang, F. Chen, M. Bai, Y. Liang, H. Wang, D. Zhao and Y. Zhao, Sol–gel synthesis of metal-phenolic coordination spheres and their derived carbon composites, *Angew. Chem., Int. Ed.*, 2018, **57**, 9838–9843, DOI: 10.1002/anie.201805781.

28 C. Chen, Y. Hao, Y. Xiao and Q. Ma, Tannic acid: a crosslinker leading to versatile functional polymeric networks: a review, *RSC Adv.*, 2022, **12**, 7689–7711, DOI: 10.1039/D1RA07657D.

29 Y. Zhang, E. Villarreal, G. G. Li, W. Wang and H. Wang, Plasmonic nanozymes: engineered gold nanoparticles exhibit tunable plasmon-enhanced peroxidase-mimicking activity, *J. Phys. Chem. Lett.*, 2020, **11**, 9321–9328, DOI: 10.1021/acs.jpclett.0c02640.

30 R. Cai, X. Gao, C. Zhang, Z. Hu, Y. Ji, J. Liu and X. Wu, Improving peroxidase activity of gold nanorod nanozymes by dragging substrates to the catalysis sites *via* cysteine modification, *Nanotechnology*, 2021, **32**, 485702, DOI: 10.1088/1361-6528/ac1e53.

31 S. Morisada, Y. H. Kim, T. Ogata, Y. Marutani and Y. Nakano, Improved ADSORPTION BEHAVIORS OF AMINE-MODIFIED TANNIN GEL FOR PALLADIUM AND PLATINUM IONS IN ACIDIC CHLORIDE SOLUTIONS, *Ind. Eng. Chem. Res.*, 2011, **50**, 1875–1880, DOI: 10.1021/ie102193a.

32 F. L. Braghiroli, V. Fierro, M. T. Izquierdo, J. Parmentier, A. Pizzi and A. Celzard, Nitrogen-doped carbon materials produced from hydrothermally treated tannin, *Carbon*, 2012, **50**, 5411–5420, DOI: 10.1016/j.carbon.2012.07.027.

33 C. Zhang, X. Zhang, Y. Ye, P. Ni, C. Chen, W. Liu, B. Wang, Y. Jiang and Y. Lu, Manganese-doped iron coordination polymer nanoparticles with enhanced peroxidase-like activity for colorimetric detection of antioxidants, *Analyst*, 2022, **147**, 238–246, DOI: 10.1039/D1AN01953H.